JOURNAL OF GEOPHYSICAL RESEARCH, VOL. 111, F03011, doi:10.1029/2005JF000454, 2006



# A comparative study of detrital mineral and bedrock age-elevation methods for estimating erosion rates

Katharine W. Huntington[1] and Kip V. Hodges[1]

Received 21 December 2005; revised 15 March 2006; accepted 17 April 2006; published 9 September 2006.

[1] The age-elevation pattern of thermochronologic data has been used for many years to estimate apparent erosion rates in orogenic settings. Recently, it has been suggested that thermochronologic data for detrital minerals from active river system sediments can be used as an effective proxy for bedrock age-elevation distributions, serving as an alternative method for erosion rate studies. This ''detrital mineral thermochronology'' (DMT) method is easier, faster, and more cost-effective than the traditional bedrock approach, and provides additional information about transients in topography and sediment delivery that may vary on diurnal to millennial timescales for a particular sampling site. However, two variants of the DMT method have been described in the literature, and they can yield very different erosion rate estimates. We tested both of these approaches against the traditional age-elevation method using detrital and bedrock $^{40}Ar/^{39}Ar$ muscovite data sets from a single river catchment in the Annapurna Range, Nepal Himalaya. A nominal erosion rate estimate of ~0.6 km/Myr for the 5.0–2.5 Ma period was calculated from the bedrock data, presented here for the first time. This result agrees with the ~0.7 km/Myr (maximum) estimate from the detrital data set, which was derived from the DMT variant that emphasizes the range of single-grain ages for a detrital sample, in this case, 11–2.5 Ma. However, the other DMT variant, which emphasizes the mean of the sample age distribution, yields an erosion rate estimate of ~2.3 km/Myr. The simplest explanation for this discrepancy is that erosion rate increased significantly after ~2.5 Ma, a scenario that is supported by apatite fission track data from the catchment.

**Citation:** Huntington, K. W., and K. V. Hodges (2006), A comparative study of detrital mineral and bedrock age-elevation methods for estimating erosion rates, *J. Geophys. Res.*, *111*, F03011, doi:10.1029/2005JF000454.

## 1. Introduction

[2] The relationship between bedrock cooling age and sample elevation is frequently used as a proxy for long-term erosional exhumation rate [e.g., *Wagner and Reimer*, 1972; *Foster and Gleadow*, 1996; *Brandon et al.*, 1998; *Crowley et al.*, 2002; *Reiners et al.*, 2002; *Balestrieri et al.*, 2003; *Bartolini et al.*, 2003; *Ducea et al.*, 2003; *House et al.*, 2003; *Reiners et al.*, 2003; *Thiede et al.*, 2004]. Unfortunately, limited outcrop or access may restrict bedrock sample collection, and because analyses are costly and time-consuming, information from a small number of samples must often be used to represent a large area. Recently, workers have sought to avoid these limitations by using detrital mineral samples from modern rivers that integrate bedrock muscovite $^{40}Ar/^{39}Ar$ cooling ages from the contributing area [*Brewer et al.*, 2003, 2006; *Ruhl and Hodges*, 2005; *Hodges et al.*, 2005]. Building on a suggestion first made by *Stock and Montgomery* [1996], this ''detrital mineral thermochronology'' (DMT) method assumes that the distribution of single-grain cooling ages in a sedimentary sample accurately reflects the distribution of bedrock cooling ages with elevation and thus can be inverted for an estimate of cooling rate. Theoretically, the DMT estimate should be comparable to an estimate made more conventionally from bedrock age-elevation data, but the DMT approach has some added benefits. First, it is an efficient way to determine patterns in erosion rate at a variety of length scales, which can then be used to infer the direction and magnitude of changes in relief over time [*Braun*, 2002]. Second, DMT analysis of stored sediments in fluvial terraces can provide valuable insights regarding changes in the erosional history of specific catchments over millennial timescales.

[3] Despite the potential power of this approach, it is a matter of concern that the two published variants of the method [*Brewer et al.*, 2003, 2006; *Ruhl and Hodges*, 2005; *Hodges et al.*, 2005] have been shown to yield erosion rate estimates that vary by more than a factor of 3 when applied to the same $^{40}Ar/^{39}Ar$ detrital muscovite data set from the Nyadi Khola catchment in the Annapurna Range of central Nepal [*Ruhl and Hodges*, 2005]. Here we investigate the two variants by comparing the estimates they provide with a newly reported conventional estimate based on age-elevation data from bedrock samples collected in the Nyadi Khola catchment. We show that the *Ruhl and Hodges* [2005] variant of the DMT method yields a higher-fidelity

[1]Department of Earth, Atmospheric and Planetary Science, Massachusetts Institute of Technology, Cambridge, Massachusetts, USA.


0148-0227/06/2005JF000454$09.00

**Table 1.** Comparison of DMT-R and DMT-B Methods and Assumptions

| | DMT-B | DMT-R |
|---|---|---|
| Time period for erosion rate estimate | time period from the time represented by the oldest sample date to the present | time interval represented by the range of sample dates, or "closure interval" |
| Spatial extent for erosion rate estimate | the entire contributing area, or catchment | the entire contributing area, or catchment |
| Summary of method for estimating erosion rate | 1. Analyze large number of single grains from detrital sediment sample collected in modern channel.<br>2. Model $T_C$ isotherm depth beneath catchment as a function of rock thermal properties and a spatially uniform, constant in time erosion rate.<br>3. Use prescribed erosion rate from thermal model to define model age-elevation gradient.<br>4. Combine age-elevation gradient, closure isotherm depth from thermal model, and catchment's hypsometry to create synthetic cooling-age distribution.<br>5. Repeat process for an array of rates.<br>6. Select preferred rate estimate as that which minimizes misfit between observed and synthetic cooling-age distribution. | 1. Analyze large number of single grains from detrital sediment sample collected in modern channel.<br>2. Estimate erosion rate from the ratio of catchment relief (total elevation difference in contributing area) to age range observed in detrital sample:<br>$E = R/t_{range}$<br>3. Test assumptions (see below). |
| Required Assumptions: | | |
| (1) Representative sampling | (1) Detrital sample represents bedrock in proportion to area. (Implicit in this assumption is assumption of spatially uniform modern erosion and assumption of uniform target mineral distribution.) | (1) Detrital sample represents bedrock in proportion to area. (Implicit in this assumption is assumption of spatially uniform modern erosion and assumption of uniform target mineral distribution.) |
| (2) Erosion in space (topographic steady state) | (2) Catchment's long-term (million-year timescale) erosion is spatially uniform from the beginning of closure interval to the present, and erosion is spatially uniform at time of sample collection. | (2) Catchment's long-term (million-year timescale) erosion is spatially uniform from the beginning of closure interval to the present, and erosion is spatially uniform at time of sample collection. |
| (3) Erosion through time (thermal steady state) | (3) Erosion rate is constant from beginning of closure interval to the time of sample collection. | (3) Erosion rate is constant during closure interval, but rate may vary afterwards. |
| (4) $T_C$ isotherm geometry | (4) $T_C$ isotherm is approximately horizontal over topographic wavelength of interest. | (4) $T_C$ isotherm is approximately horizontal over topographic wavelength of interest. |
| (5) $T_C$ isotherm depth | (5) $T_C$ isotherm is at constant depth from the beginning of the closure interval to the time of sample collection. $T_C$ isotherm depth from thermal model must be the same as the actual $T_C$ isotherm depth. | (5) $T_C$ isotherm is at constant depth during the closure interval, and depth may vary afterwards. Actual $T_C$ isotherm depth does not need to be assumed. |
| (6) Particle paths | (6) Rocks follow vertical particle trajectories; if not, thermal model is not appropriate. | (6) Rocks follow vertical particle trajectories; if not, relative estimates still good. |
| Tests of assumptions | 1. No direct test of model assumptions available.<br>2. Poor fit of best-fit synthetic cooling-age distribution to observed distribution qualitatively indicates that one or more model assumption has been violated.<br>3. Comparison of best-fit model and observed distribution does not provide a test of the accuracy of the $T_C$ isotherm depth estimate. | 1. Statistical tests are available to evaluate the mismatch between the observed cooling-age distribution and the catchment's hypsometric curve.<br>2. Significant mismatch between cooling-age distribution and hypsometric curve indicates that one or more model assumption has been violated. |

proxy for the conventional estimate in this instance. The discrepancy between the two DMT variants is likely due to a late acceleration in bedrock exhumation rate that is not recorded directly in the age-elevation relationships derived from the detrital or bedrock data sets. This rate change has different implications for the two methods because they require different assumptions to hold over different time intervals. This distinction implies that each method is useful in its own way, and the application of both can provide important information regarding temporal changes in bedrock erosion rate that may reflect changes in climate or deformational kinematics.

## 2. Detrital Thermochronology as a Proxy for Age-Elevation Profiles

[4] Since temperature is known to increase with depth in the stable continental crust, cooling ages from thermochronologic studies can reflect the way rocks changed position with respect to Earth's surface through time [*Purdy and Jaeger*, 1976; *Wagner et al.*, 1977]. For the $^{40}Ar/^{39}Ar$ muscovite thermochronometer, the cooling age roughly corresponds to the time at which a sample cooled below a bulk closure temperature of ~350°C [*Hames and Bowring*, 1994; *Hodges*, 2003]. The traditional bedrock age-elevation approach for determining exhumation rates from cooling ages exploits the difference in elevation between valleys and ridges and its effect on bedrock cooling age distributions at the surface [*Wagner and Reimer*, 1972; *Wagner et al.*, 1977; *Fitzgerald and Gleadow*, 1988]. This elevation difference results in longer exhumation paths from the closure isotherm depth to points on the surface on ridges than to points in valleys, such that bedrock cooling ages are expected to increase with elevation in proportion to the exhumation rate. In order to apply this approach, bedrock samples are collected over a range of elevations, and the apparent

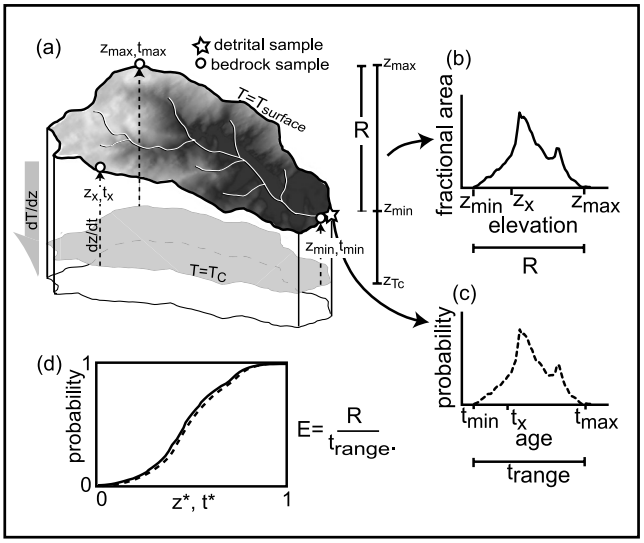


**Figure 1.** Schematic diagram outlining method of *Ruhl and Hodges* [2005] for estimating long-term catchment-averaged erosion rates using the distribution of detrital mineral cooling ages from modern stream sediment and the hypsometry of the contributing catchment: R is the total catchment relief, and $t_{range}$ is the cooling-age range. (a) Here dT/dz indicates increase of temperature with depth beneath the catchment, and dz/dt denotes the erosion rate. A detrital sample from the catchment outlet (star) represents bedrock in proportion to surface area in the contributing catchment. Bedrock (open circle) at the lowest elevation ($z_{min}$) has the shortest exhumation path from the closure temperature isotherm at depth $z_{Tc}$ where $T = T_C$ to the surface ($T = T_{surface}$), and thus represents the minimum cooling age in the catchment ($t_{min}$). A bedrock grain at the highest elevation ($z_{max}$) has the longest exhumation path and oldest cooling age ($t_{max}$), and bedrock grains from intermediate elevations ($z_x$) have cooling ages ($t_x$), where $t_{min} < t_x < t_{max}$. (b) Hypsometric curve is determined from the catchment digital elevation model (DEM). (c) Cooling-age synoptic probability density function (SPDF) is used to describe detrital cooling age distribution for single-grain analyses. (d) Cumulative SPDFs (CSPDFs) are shown for cooling age (dashed curve) and elevation (solid curve). Normalized cooling age, t* (equal to the difference between the observed age and minimum age divided by $t_{range}$), and normalized elevation, z* (equal to the difference between the observed elevation and minimum elevation divided by R), as described in equations (9a) and (9b) of *Ruhl and Hodges* [2005], are plotted on the abscissa. Apparent erosion rate $E = R/t_{range}$.

exhumation rate over the time period represented by the range of sample cooling ages is defined as the inverse of the age-elevation gradient. For a given increase in elevation, the age increase is smaller for faster erosion rates and larger for slower erosion rates.

[5] Detrital thermochronology of modern and ancient sediments has been demonstrated to be a powerful tool for establishing sedimentary provenance, lag-time histories, erosional patterns, and relative erosion rates [e.g., *Bernet and Garver*, 2005; *Hodges et al.*, 2005]. As an alternative to the bedrock age-elevation technique, two methods for determining catchment-wide exhumation rates from detrital mineral thermochronology of modern river sediment also have been described (Table 1). While both of these methods were developed for the analysis of muscovite $^{40}Ar/^{39}Ar$ data, they are equally valuable interpretive tools for fission track or (U-Th)/He detrital thermochronologic data sets. In the approach of *Brewer et al.* [2003, 2006] (hereafter referred to as DMT-B) a thermal model is used to predict the distribution of cooling ages in a catchment as a function of a closure depth model, catchment hypsometry, relief, and erosion rate. The best-fit erosion rate estimate from the time the sample cooled through the closure temperature to the present is found when the mismatch between the model cooling-age distribution and measured detrital sample cooling-age distribution is minimized, essentially when the bulk of the detrital age distribution coincides with the average age of the modeled distribution.

[6] *Stock and Montgomery* [1996] speculated that the range of ages given by single-grain analyses from an ancient detrital sample might be used to establish the total paleo-relief of the sediment source region if the exhumation rate were known. *Ruhl and Hodges* [2005] pointed out how this same logic could be used to invert detrital data from modern catchments for bedrock erosion rate during the time period represented by the range of sample dates:

$$E = R/t_{range}, \quad (1)$$

where $E$ is apparent erosion rate, $R$ is upstream catchment relief, and $t_{range}$ is the range of detrital mineral cooling ages (Figure 1). We will refer to this variant of the DMT method as DMT-R.

[7] A series of assumptions is implicit in each of these variants of detrital mineral thermochronology. A complete list of these assumptions, along with a summary of DMT-B and DMT-R methods for estimating erosion rates, can be found in Table 1. Both DMT-B and DMT-R assume vertical rock particle trajectories, spatially uniform erosion rates across the catchment, insignificant sediment transport and storage times within the system, and representative sampling of the catchment's bedrock in the detrital sample. In addition, DMT-B assumes a specific geothermal gradient, constant erosion rate from the time of closure to the present, and thermal and topographic steady state through time. In contrast, DMT-R assumes a constant erosion rate and thermal and topographic steady states for the catchment only during the time period represented by the range of sample dates, or the "closure interval." *Ruhl and Hodges* [2005] describe how the most important of these assumptions can be evaluated through empirical thermochronologic studies and through the comparison of a catchment's detrital cooling age and area-elevation (hypsometric) distributions (Figure 1d and Table 1).

[8] On the basis of such comparisons, *Ruhl and Hodges* [2005] were able to say with some confidence that one detrital suite from a 200 $km^2$ drainage in the Annapurna Range of central Nepal (Nyadi Khola catchment) yielded results consistent with the necessary assumptions and therefore should provide a robust erosion rate estimate over the $\sim$11–2.5 Ma period. However, their erosion rate estimate

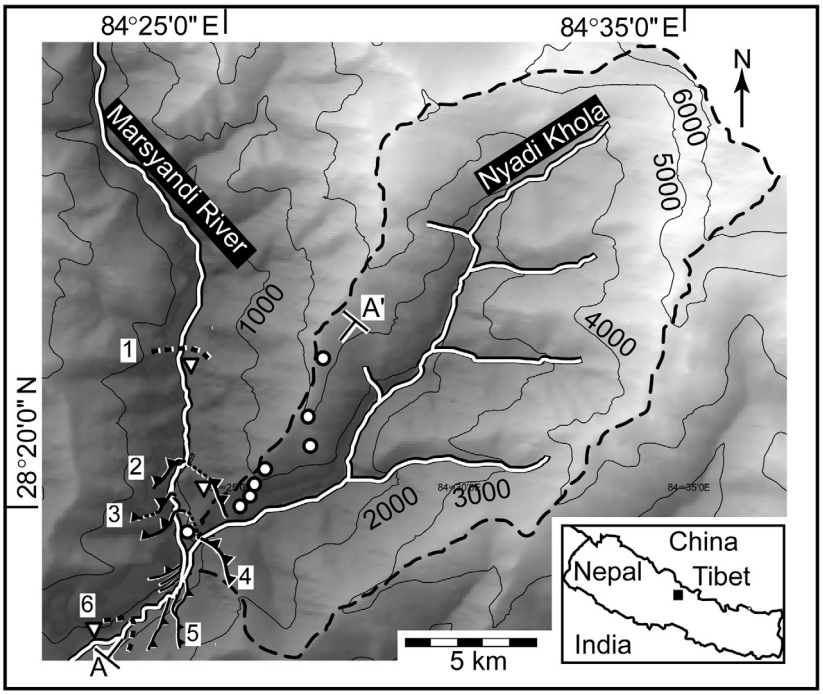


**Figure 2.** Simplified structural map of area near confluence of the Nyadi and Marsyandi Rivers. Inset shows location of study area, roughly 120 km to the northwest of the Kathmandu basin. Base map is 90-m DEM draped over a hillshade map. Nyadi catchment is outlined with a black dashed line. Map symbols: bedrock $^{40}Ar/^{39}Ar$ sample locations (white circles); from north to south, towns of Ghemu, Bahundada and Bhulbhule (white inverted triangles); structures as mapped by *Hodges et al.* [2004], with black lines with triangles indicating faults (dashed where inferred), labeled with numbers in white boxes: 1, northern limit of low-temperature shear zone; 2, Nalu thrust, the major fault strand of the Main Central Thrust in this area; 3, Arkhale thrust; 4, Usta thrust; 5, Nadi thrust; and 6, southern limit of low-temperature shear zone. Line of section A to A′ refers to Figure 3.

was much slower than the rate estimated by *Brewer et al.* [2006] for the same drainage using the DMT-B variant that requires a constant erosion rate from ~11 Ma to the present. In order to better understand which approach more reliably represents the rate that might result from a conventional bedrock age-elevation dating campaign, we elected to conduct the latter in the Nyadi Khola drainage.

## 3. Sampling Strategy

[9] The Nyadi Khola catchment, a tributary of the Marsyandi River, is located roughly 120 km to the northwest of the Kathmandu basin (Figure 2). This position coincides with the physiographic transition between the rugged Higher Himalayan ranges containing 7000–8000 m peaks and the more subdued Lower Himalayan foothills immediately to the south [*Hodges et al.*, 2001; *Wobus et al.*, 2003; *Hodges et al.*, 2004; *Wobus et al.*, 2005]. Geomorphic [*Seeber and Gornitz*, 1983; *Wobus et al.*, 2003; *Hodges et al.*, 2004] and geodetic [*Jackson and Bilham*, 1994a, 1994b; *Bilham et al.*, 1997] studies indicate that the Higher Himalayan ranges are being uplifted relative to the Lower Himalayan foothills, although exactly how deformational structures relate to this differential movement remains a topic of debate [*Cattin and Avouac*, 2000; *Hodges et al.*, 2004].

[10] *Hodges et al.* [2004] mapped the area near the confluence of the Nyadi and the Marsyandi rivers in detail, and divided the local bedrock into three units, each rich in our target mineral muscovite: (1) the pelitic gneisses and granites of the Bahundada unit; (2) the underlying pelitic schists, granitic orthogneisses, marbles, and quartzites of the Siurun Complex; and (3) the structurally lowest Kuncha Schist, composed of pelitic schists and phyllites similar in composition to the schists of the Siurun Complex. At the regional scale, the Bahundada gneiss correlates with the traditionally defined Greater Himalayan Sequence [*Le Fort*, 1975; *Hodges*, 2000], whereas the Kuncha and Siurun units are both part of the Lesser Himalayan Sequence [*Gansser*, 1964; *Stöcklin*, 1980; *Valdiya*, 1980]. The Siurun-Bahundada contact, or Nalu Thrust (Figures 2 and 3), corresponds to the principal fault of a major Himalayan fault system, the Main Central Thrust (MCT) system as defined in Nepal by a variety of workers [*Colchen et al.*, 1986; *Pêcher*, 1989; *Coleman and Hodges*, 1998; *Hodges et al.*, 2004]. Breaking with tradition, *Martin et al.* [2005] suggested that the principal thrust of the MCT system in this area was actually a structure roughly 1 km south of the trace of the Nalu Thrust. This interpretation was not based on structural observations or a lithologic discontinuity, but instead on a discontinuity in the Nd isotopic characteristics of samples collected north and south

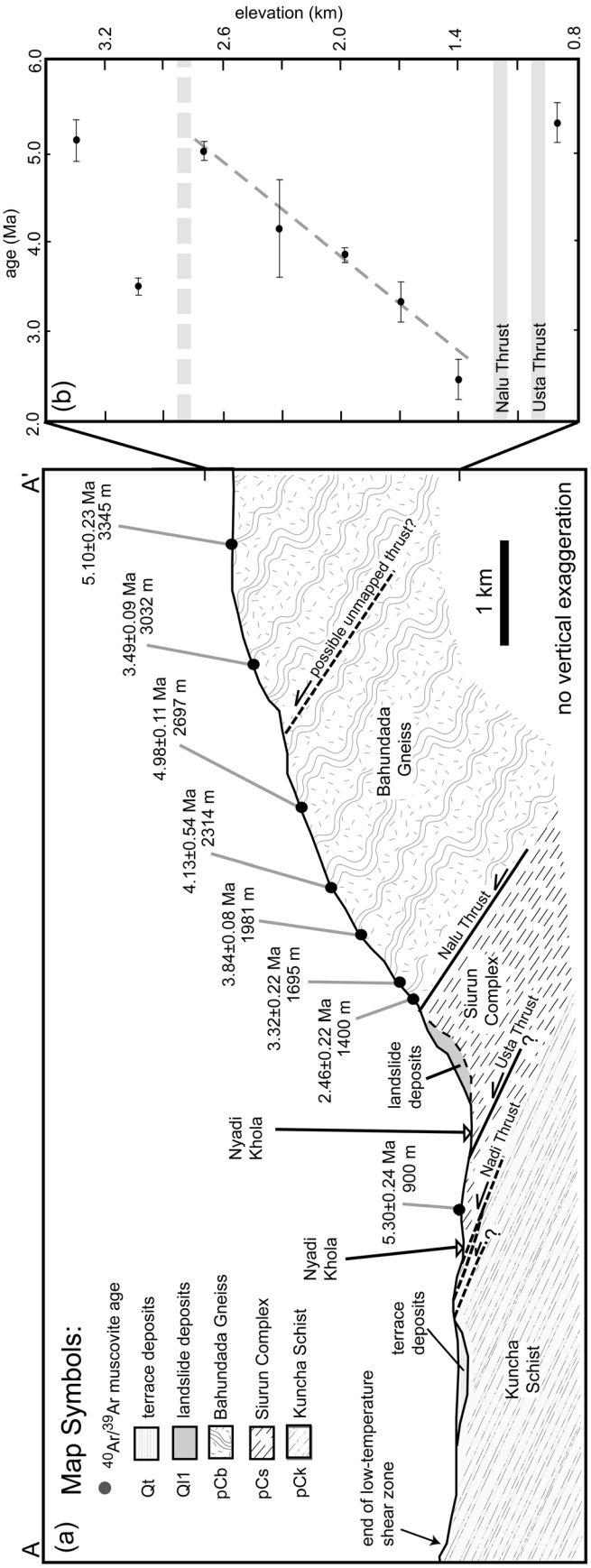


**Figure 3.** Bedrock sample locations in the context of mapped structures. (a) Cross section with $^{40}Ar/^{39}Ar$ muscovite bedrock sample locations (circles) from this study. Age in millions of years with 2σ analytical uncertainty and sample elevation in meters. (b) Bedrock muscovite $^{40}Ar/^{39}Ar$ cooling age with 2σ uncertainties plotted versus sample elevation. Least squares linear regression of the 1400 m to 2697 m data, with elevation as the dependent variable, yields an erosion rate estimate of ~0.6 km/Ma (0.57 ± 0.05 km/Myr (2σ); error-weighted best-fit line dashed through data).

of that specific position in the tectonic stratigraphy. Previously, *Hodges et al.* [2004] had mapped a ~30° north-dipping thrust fault (the Usta Thrust) at approximately that position. In the Marsyandi Valley, the MCT system was an active tectonic feature by the Early Miocene [*Coleman and Hodges*, 1998], but the occurrence of ductile shear fabrics as young as Pliocene [*Edwards*, 1995; *Catlos et al.*, 2001], as well as brittle faults and breccia zones [*Hodges et al.*, 2004], imply a long history of faulting at a variety of structural levels. Of particular importance to our study is the evidence cited by *Hodges et al.* [2004] for some amount of Pleistocene slip on the Nalu Thrust, the Usta Thrust, and other faults within the physiographic transition from the Higher to the Lower Himalaya. Hodges and colleagues considered the Nalu, Usta, and one other fault, the structurally lower Nadi Thrust (Figures 2 and 3), as the most likely structures to have experienced significant Pleistocene slip, but poor exposure and the existence of a broad zone of brittle shearing allow the possibility that there are other important (but unmapped) Quaternary thrust faults in the area (Figure 2).

[11] Previously published bedrock $^{40}Ar/^{39}Ar$ results for the region [*Copeland et al.*, 1991; *Macfarlane et al.*, 1992; *Macfarlane*, 1993; *Edwards*, 1995; *Catlos et al.*, 2001; *Bollinger et al.*, 2004] are in broad agreement with the detrital cooling ages documented by *Ruhl and Hodges* [2005] and *Brewer et al.* [2006]. However, none of these data were collected along a single age-elevation profile over a lateral distance short enough to ensure that the erosion rate estimate that could be made from such data was insensitive to the effects of topography on isotherm geometry [*Braun*, 2002]. Unfortunately, there is no easily accessible part of the Nyadi Khola drainage that is not crossed by the swarm of Quaternary faults mapped by *Hodges et al.* [2004]. We present here $^{40}Ar/^{39}Ar$ muscovite data for bedrock samples collected along a steep ridge transect, near the confluence of the Nyadi Khola and the Marsyandi, over elevations that range from 900 to 3345 m (Figure 2). The lowest elevation sample in this suite (from the Siurun Complex) and the second lowest (at 1400 m) are separated by both the Usta and Nalu Thrusts. Seven samples (1400 m to 3345 m) were collected from the Bahundada Gneiss. The four lowest of these are from the steepest part of the transect and are likely to represent a structurally contiguous block. The three highest samples were collected a significant map distance away from the others and their structural relationships are less clear.

## 4. $^{40}Ar/^{39}Ar$ Thermochronology Methods and Results

[12] Bedrock $^{40}Ar/^{39}Ar$ ages and sample elevations are summarized in Table 2. Aliquots rich in muscovite were prepared from each bedrock sample using standard magnetic and gravimetric techniques. For each sample, 30–50 mg of muscovite separate was hand picked to ensure 99.9% purity. The grains were washed in distilled water and ethanol and packaged in copper foil prior to irradiation at the McMaster University nuclear reactor in Ontario, Canada. Values for the irradiation parameter $J$ were determined using Taylor Creek sanidine at 27.92 Ma [*Dalrymple and Duffield*, 1988; *Renne et al.*, 1998] as the flux monitor. Corrections for interfering reactions were measured using a combination of synthetic and natural salts [*Kirby et al.*, 2002]. Step-heating experiments were carried out for samples 01NL02, 01NL04, 01NL05, 01NL06, and 01NL08 at the noble gas laboratory at the Massachusetts Institute of Technology (MIT), and total-fusion analyses were carried out for samples NBE-4, 01NL03, and 01NL07 at the Scottish Universities Environmental Research Center (SUERC).

[13] At MIT, samples were heated incrementally in a double-vacuum furnace. After purification, Ar isotopic ratios for each step were measured on an MAP 215-50 mass spectrometer using an electron multiplier detector and blank corrected. Dates for each increment were determined and 2σ apparent age uncertainties were assigned using the program ArArCALC version 2.2 [*Koppers*, 2002]. The step-heating data with 2σ uncertainties are reported in Table S1 in the auxiliary material[1]. Apparent-age release spectra (cumulative percent potassium-derived $^{39}Ar$ released versus apparent age) and inverse isotope correlation plots ($^{39}Ar/^{40}Ar$ versus $^{36}Ar/^{40}Ar$) are shown in Figure S1 in the auxiliary material. In this paper, a "plateau" in one of these spectra is defined as comprising three or more contiguous steps that overlap with the mean at the 2σ level of error excluding the error contribution from the irradiation parameter $J$, with a total minimum $^{39}Ar_K$ release of 60%. Steps with less than 20% radiogenic $^{40}Ar$ were not considered. Plateau ages for samples in this study comprised a minimum of 70% of the total $^{39}Ar_K$ released, and were calculated as the weighted mean of ages of steps on the plateau, with each step age weighted by the inverse of its variance.

[14] Total-fusion analyses at SUERC were done using a modified double-vacuum resistance furnace. Each sample was heated for 30 min (15 min at 950°C followed by 15 min at 1400°C). After the resulting gas was purified, Ar isotopic ratios were measured on an MAP 215-50 mass spectrometer using a Faraday detector. Following blank corrections, dates were determined and 2σ apparent age uncertainties were assigned using the program ArArCALC version 2.2 [*Koppers*, 2002]. The total-fusion results with 2σ uncertainties are reported in Table S1 in the auxiliary material. Ages for step-heating and total-fusion experiments summarized in Table 2 range from 2.46 ± 0.22 Ma (2σ) to 5.30 ± 0.24 Ma.

## 5. Bedrock and DMT Estimates of Erosion Rate

[15] Bedrock muscovite $^{40}Ar/^{39}Ar$ age is plotted against structural position and sample elevation in Figure 3. Cooling ages of the four samples collected from the apparently coherent block between 1400 m and 2314 m increase smoothly with elevation, and the same age-elevation trend appears to extend to include the 2697 m sample with a cooling age of 4.98 ± 0.11 Ma. A linear regression of the elevations of these five samples against their cooling ages suggests an erosion rate of 0.6 km/my over the ~5.0 to ~2.5 Ma time range. However, this simple pattern is apparently complicated by faulting at structurally lower and higher levels. The one sample collected beneath the

[1] Auxiliary material data sets are available at ftp://ftp.agu.org/apend/jf/2005jf000454. Other auxiliary material files are in the HTML.

**Table 2.** Summary of Bedrock Muscovite $^{40}Ar/^{39}Ar$ ages (Ma) with 2σ Uncertainty Including the Uncertainty in the Irradiation Parameter J[a]

| Sample Name | Elevation, m | Age, Ma | Experiment Type |
|---|---|---|---|
| NBE-4 | 900 | 5.30 ± 0.24 | total fusion after degassing step |
| 01NL02 | 1400 | 2.46 ± 0.22 | step-heating plateau |
| 01NL03 | 1695 | 3.32 ± 0.22 | total fusion after degassing step |
| 01NL04 | 1981 | 3.84 ± 0.08 | step-heating plateau |
| 01NL05 | 2314 | 4.13 ± 0.54 | step-heating plateau |
| 01NL06 | 2697 | 4.98 ± 0.11 | step-heating plateau |
| 01NL07 | 3032 | 3.49 ± 0.09 | total fusion after degassing step |
| 01NL08 | 3345 | 5.10 ± 0.23 | step-heating plateau |

[a]Sample elevation (m) and experiment type are also noted.

Usta and Nalu thrusts has a muscovite cooling age of 5.30 ± 0.24 Ma, but the age of the structurally lowest sample in the Nalu Thrust hanging wall is only 2.46 ± 0.22 Ma. This disruption is consistent with post-2.46 Ma offset of either the Nalu Thrust, the Usta Thrust, or both. The two highest samples yield cooling ages that are younger than the age-elevation trend of the 1400 m to 2697 m samples would predict. We speculate that this inconsistency may be related to an unmapped, N-dipping thrust (Figure 3a). Future detailed mapping of the ridge between the elevations of 2697 and 3032 m might serve as a test of this hypothesis.

[16] Such structural complications notwithstanding, the 0.6 Ma apparent erosion rate derived from the 1400 m to 2697 m bedrock data can be compared with the results of previous DMT studies by *Brewer et al.* [2006] and *Ruhl and Hodges* [2005]. The DMT-R estimate (0.7 km/Myr), a maximum value, is entirely consistent with the conventional bedrock estimate. (While the analytical uncertainty on individual grain ages tends to increase the apparent age range represented by a detrital sample, underestimation of the extremes of the distribution due to limited sample size tends to decrease the apparent age range. The DMT-R method accounts for the tendency of the analytical uncertainty to overestimate the age range. Thus, because of finite sample size, the resulting age range is a minimum value, making the erosion rate a maximum estimate). However, the DMT-B estimate (2.3 km/Myr) is very different. We believe that the cause of this inconsistency can be traced to differences between the sets of assumptions required by the DMT-R and DMT-B methodologies, and the time periods over which each method aims to estimate erosion rates, discussed in detail below.

## 6. A Comparison of the DMT-B and DMT-R Techniques

[17] The difference in erosion rates estimated by *Brewer et al.* [2006] and *Ruhl and Hodges* [2005] cannot be attributed to a difference in the cooling-age distributions used to represent the Nyadi catchment bedrock, as the distributions used in the two studies are statistically indistinguishable (Figure 4a). Instead, the approach of *Brewer et al.* [2006] differs from that of *Ruhl and Hodges* [2005] in two important ways that could account for the fact that the DMT-B estimate does not agree with the conventional bedrock estimate while the DMT-R estimate does. First, the DMT-B result depends on an ad hoc thermal model, the accuracy of which, unfortunately, is unavoidably difficult to evaluate in rapidly eroding mountainous regions. Second, the DMT-B approach requires more restrictive assumptions than the DMT-R approach. For the Nyadi case, a particularly important assumption is that the erosion rate in the catchment has been constant from the beginning of the age range in the detrital sample (in this case, 11 Ma) to the present.

[18] *Brewer et al.* [2003, 2006] modeled the thermal structure beneath the Nyadi catchment as a function of rock thermal properties and a constant, spatially uniform erosion rate. In their forward model, this prescribed rate defines the synthetic catchment's bedrock age-elevation gradient. The age-elevation gradient, closure isotherm depth from the thermal model, and catchment's hypsometry are then used to create a synthetic detrital cooling-age distribution (Figure 4b). This process is repeated for an array of erosion rates, and the preferred rate estimate is that which minimizes the misfit between the synthetic cooling-age distribution and the sample cooling-age distribution. Unfortunately, rock thermal properties and heat flow estimates vary greatly in mountainous regions [e.g., *Ehlers*, 2005], and it is impossible to evaluate a priori whether or not the boundary condition and configuration of a particular thermal model faithfully reproduce the thermal structure beneath a particular catchment since the closure interval. Moreover, it is likely that different model erosion rates could produce the same predicted age peak when combined with a different set of thermal parameters.

[19] Using the DMT-B approach, the best-fit synthetic age distribution for the Nyadi catchment correctly matches the location of the sample's main age peak at ~5 Ma if the erosion rate is 2.3 km/Myr (Figure 4b). However, this model does not accurately reproduce the sample's cooling age range; if the rate of erosion had been a constant 2.3 km/Myr for the past 11 Myr, the range of muscovite cooling ages in the Nyadi catchment should be no more than about 3 Myr. The observed 8.5 Myr age range invalidates this assumption, which is essential to the DMT-B approach. In contrast, the DMT-R erosion-rate estimate of *Ruhl and Hodges* [2005] does not require a constant erosion rate for the period of time not represented by the sample cooling ages, nor does it require an a priori assumption of the closure isotherm depth. Perhaps the most important difference between the two methods is our ability to evaluate the assumptions upon which each relies. In this case, the qualitative observation that the best-fit thermal model age range from the DMT-B approach is much narrower than the observed age range in the sample. This observation indi-

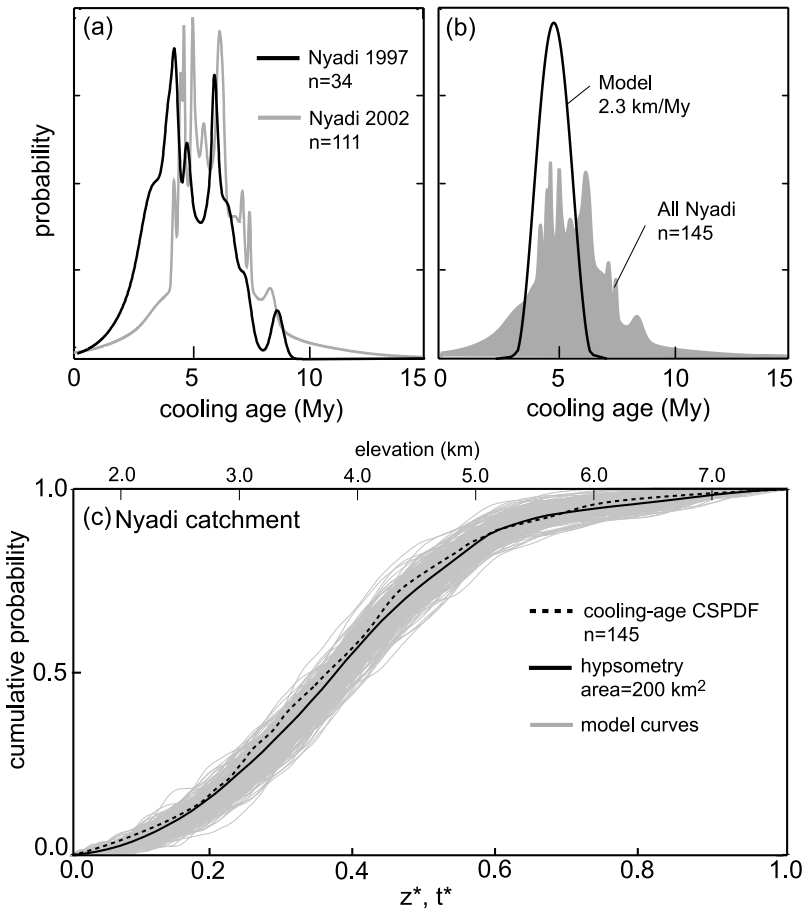


**Figure 4.** Detrital muscovite $^{40}Ar/^{39}Ar$ thermochronology for the Nyadi catchment. (a) Synoptic probability density functions (SPDF) representing the Nyadi catchment detrital cooling age signal measured by *Brewer et al.* [2006], n = 35 (gray curve), and *Ruhl and Hodges* [2005], n = 111 (black curve). The two SPDFs are statistically indistinguishable according to the Kuiper equality test, and the difference between them can be attributed to a difference in sample size and analytical precision [*Ruhl and Hodges*, 2005]. (b) Modeled best-fit synthetic SPDF of *Brewer et al.* [2006] (black curve) and observed detrital cooling-age signal for all available data (gray shaded area). Synthetic SPDF approximately fits the main peak of the observed cooling-age distribution, but is too narrow to fit the tails of the distribution [*Brewer et al.*, 2006]. (c) Cumulative SPDF (CSPDF) of observed cooling-age distribution shown in Figure 4b (dashed black curve) and observed hypsometry for the Nyadi catchment (solid black curve), plotted with 300 model simulations (solid gray curves) after *Ruhl and Hodges* [2005]. The R and $t_{range}$ values define an average age-elevation relationship of ~0.7 km/Myr for the catchment. This result is a maximum estimate for the time period represented by the sample ages. The observed cooling-age CSPDF falls easily within the range of model curves, providing strong evidence that this age-elevation relationship is robust.

cates that the assumption of a constant erosion rate from ~11 Ma to the present does not hold. However, even if the model fit both the mean age and age range of the observed distribution, if the closure-isotherm depth estimate is wrong, the rate estimate will be wrong; in this case there would be no way to evaluate the accuracy of the result. In contrast, using the comparison of detrital cooling-ages and hypsometry, it is possible to evaluate the assumptions required by the DMT-R approach (e.g., Figure 4c and Table 1). If bedrock cooling age in the catchment increases linearly with elevation and the detrital mineral sample represents the catchment's cooling-age signal in proportion to area, the ratio of relief to detrital age range is analogous to the elevation-age gradient that would be given by a traditional bedrock age-elevation study. It is possible to evaluate these assumptions because a strong correlation of hypsometry and cooling ages is expected if they are valid. As a consequence, a significant mismatch between the hypsometric curve and detrital mineral cooling-age distribution indicates that one or more assumptions have been violated [*Ruhl and Hodges*, 2005]. For the Nyadi catchment, cooling age is well-correlated with hypsometry (Figure 4c), so there is no reason to suspect that the erosion rate estimate of ~0.7 km/Myr over the interval from ~11 to 2.5 Ma determined by *Ruhl and Hodges* [2005] would not be consistent with the results of a traditional bedrock age-elevation study.

The favorable correlation of detrital cooling-age signal and hypsometry further suggests that the 0.6 km/Myr bedrock result is a robust rate estimate, not only for the limited elevations and ~5.0 to 2.5 Ma time interval represented by the bedrock samples, but for the full relief of the catchment and entire age range represented by the detrital sample from ~11 to 2.5 Ma.

## 7. Reconciliation of the DMT-B, DMT-R, and Bedrock Results

[20] Provided that all of the assumptions of the two DMT variants are correct, we might expect them both to yield consistent, and correct, estimates of erosion rate. The fact that this is not the case for the Nyadi Khola data set has important implications regarding the erosional history of the catchment. While the bedrock data confirm the DMT-R estimate for the 11-2.5 Ma interval, an erosion rate of only a few tenths of a kilometer per million years seems insufficient to bring the youngest bedrock sample from the depth of the muscovite closure isotherm (nominally 350°C) to the surface in only 2.5 Ma. The simplest explanation for the young average age and the wide age range represented by the Nyadi catchment samples is that exhumation rate increased dramatically over the Pliocene-Recent interval. Very young (<1 Ma) apatite fission track dates, representing a bulk closure temperature of ~110°–140°C for rapid cooling rates [*Hodges*, 2003], for Greater Himalayan Sequence bedrock samples from the Marsyandi drainage lend support to this interpretation [*Burbank et al.*, 2003]. Under such circumstances, the DMT-B approach would be expected to yield a result that overestimates the 11–2.5 Ma rate, underestimates the 2.5 Ma–present rate, and does not necessarily represent a geologically meaningful average rate for this time period. Nevertheless, it is generally true that large inconsistencies between DMT-B and DMT-R estimates are indicative of a late-stage change in erosion rate; if the DMT-B rate exceeds the DMT-R rate, then an acceleration in rate is indicated. This suggests that the combined use of the DMT-R and DMT-B approaches provides a powerful way to investigate the erosional history of a catchment from the beginning of the closure interval to the time the sediment sample was deposited.

## 8. Conclusions

[21] Cooling-age distributions from modern river sediments have great potential to constrain long-term erosion rates while avoiding many limitations of traditional bedrock studies. We compared two detrital mineral thermochronology approaches that are both based on the relationship between bedrock cooling age and elevation in an eroding catchment. The DMT-R approach of *Ruhl and Hodges* [2005] emphasizes the range of single-grain ages from a detrital sample, and the erosion rate over the time interval represented by the range of ages is given by the ratio of catchment relief to the age range. If assumptions regarding the topographic and thermal history of the catchment over this time interval are not valid, this rate still represents a geologically meaningful maximum estimate of the average rate for this time interval. A comparison of the catchment's cooling age distribution and hypsometry indicate the likelihood that the assumptions have been met. The DMT-B approach of *Brewer et al.* [2003, 2006] emphasizes the mean of the detrital sample age distribution, and the erosion rate from the beginning of the closure interval to the time of sample collection is a function of the mean age and the modeled closure temperature isotherm depth. If assumptions regarding the thermal and topographic history of the catchment, particularly the assumption that the erosion rate has remained constant in time, are not valid, or if the thermal model does not accurately predict the depth of the closure temperature isotherm, the rate estimate is not geologically meaningful. Although there is no direct way to evaluate the accuracy of the thermal model, comparing results for the DMT-R and DMT-B approaches may help to evaluate whether or not these assumptions or the closure temperature isotherm depth estimate are appropriate for the catchment of interest.

[22] Because the assumptions required by the DMT-B approach are more restrictive than those required by the DMT-R approach, in general, a disagreement of DMT-R and DMT-B estimates can help indicate which conditions required by the DMT-B approach have not been met. This has important implications for our ability to investigate the erosional history of a catchment after the time period represented by the sample cooling ages. In the Nyadi catchment case, the DMT-R assumptions appear to be satisfied given the good match of hypsometry and cooling ages, indicating that the erosion rate estimate for the closure interval is robust. Indeed, the rate estimate is consistent with the conventional bedrock age-elevation rates estimate over the same time period. Even if the DMT-R model assumptions were not valid, the DMT-R estimate would represent a geologically meaningful maximum value. As a consequence, the fact that the DMT-B estimate is greater than the DMT-R estimate strongly suggests that an increase in erosion rates occurred sometime after the youngest sample cooled through its closure temperature.

[23] The DMT-B approach is analogous to the bedrock thermochronology practice of assuming a closure temperature isotherm depth and estimating a rate from the ratio of the depth estimate to a single sample's age. As is the case in conventional bedrock age-elevation studies, the age-elevation gradient given by the DMT-R method provides a proxy for erosion rate during the time period represented by the range of sample ages without requiring the assumption of a particular closure temperature isotherm depth. Just as a combination of the age-elevation approach and closure temperature isotherm depth estimates can provide a more complete picture of erosion history in conventional bedrock studies, a combination of DMT-R and DMT-B approaches can be advantageous in detrital studies.

[24] In addition, because it allows the direct comparison of hypsometry and cooling age distributions, the DMT-R approach has some added benefits. Like other detrital approaches, it is time- and cost-efficient, as the entire catchment relief can be characterized with an easy-to-collect sediment sample from low elevation that represents a longer time range than most traditional bedrock age-elevation studies. However, when bedrock cooling-age patterns are determined independently, this technique also can be used to explore erosional processes for individual fluvial systems

through time and thus track the geomorphic evolution of mountainous landscapes.

## Notation

| | |
|---|---|
| R | total catchment relief, km. |
| $t_{range}$ | total range of ages given by single-grain analyses from a detrital sample, Myr. |
| $z_x$ | sample x elevation, km. |
| $t_x$ | sample x cooling age, Myr. |
| $z_{max}$ | elevation of highest point in catchment, km. |
| $z_{min}$ | elevation of lowest point in catchment, km. |
| $t_{max}$ | cooling age of sample collected at highest point in catchment, Ma. |
| $t_{min}$ | cooling age of sample collected at lowest point in catchment, Ma. |
| $T_{surface}$ | surface temperature, °C. |
| $T_c$ | closure temperature for system of interest, °C. |
| t* | normalized cooling age; equal to the difference between the observed age ($t_x$) and minimum age ($t_{min}$) divided by $t_{range}$. |
| z* | normalized elevation; equal to the difference between sample elevation ($z_x$) and minimum elevation ($z_{min}$) divided by R. |
| E | apparent erosion rate, equivalent to inverse of elevation-age gradient. |

[25] **Acknowledgments.** We thank Bill Olszewski, Xifan Zhang, and Malcolm Pringle for their laboratory expertise, and Keegan Schmidt for assistance in sample collection. The paper benefited from discussions with Kelin Whipple and from thoughtful reviews by Pete Reiners, Matthias Bernet, and Alex Densmore. This work is a product of the National Science Foundation Continental Dynamics project ''Geomorphic-Geodynamic Coupling at the Orogen Scale.''

## References

Balestrieri, M., M. Bernet, M. T. Brandon, V. Picotti, P. W. Reiners, and M. Zattin (2003), Pliocene and Pleistocene exhumation and uplift of two key areas of the Northern Apennines, *Quat. Int.*, *101–102*, 67–73.

Bartolini, C., N. D'Agostino, and F. Dramis (2003), Topography, exhumation, and drainage network evolution of the Apennines, *Episodes*, *26*(3), 212–216.

Bernet, M., and J. I. Garver (2005), Fission-track analysis of detrital zircon, *Rev. Miner. Geochem*, *58*, 315–350.

Bilham, R., K. Larson, J. Freymuller, and P. I. Members (1997), GPS measurements of present-day convergence across the Nepal Himalaya, *Nature*, *386*, 61–64.

Bollinger, L., J. P. Avouac, O. Beyssac, E. J. Catlos, T. M. Harrison, M. Grove, B. Goffé, and S. Sapkota (2004), Thermal structure and exhumation history of the Lesser Himalaya in central Nepal, *Tectonics*, *23*, TC5015, doi:10.1029/2003TC001564.

Brandon, M. T., M. K. Roden-Tice, and J. I. Garver (1998), Late Cenozoic exhumation of the Cascadia accretionary wedge in the Olympic Mountains, northwest Washington State, *Geol. Soc. Am. Bull.*, *110*, 985–1009.

Braun, J. (2002), Estimating exhumation rate and relief evolution by spectral analysis of age-elevation datasets, *Terra Nova*, *14*, 210–214.

Brewer, I. D., D. W. Burbank, and K. V. Hodges (2003), Modelling detrital cooling-age populations: Insights from two Himalayan catchments, *Basin Res.*, *15*, 305–320.

Brewer, I. D., D. W. Burbank, and K. V. Hodges (2006), Downstream development of a detrital cooling-age signal: Insights from $^{40}Ar/^{39}Ar$ muscovite thermochronology in the Nepalese Himalaya, in *Tectonics, Climate and Landscape Evolution*, *Penrose Conf. Ser.*, *Spec. Pap. 398*, pp. 321–338, doi:10.1130/2006.2398 (20), Geol. Soc. of Am., Boulder, Colo.

Burbank, D. W., A. E. Blythe, J. K. Putkonen, B. A. Pratt-Sitaula, E. J. Gabet, M. E. Oskin, A. P. Barros, and T. P. Ojha (2003), Decoupling of erosion and precipitation in the Himalaya, *Nature*, *426*, 652–655.

Catlos, E. J., T. M. Harrison, M. J. Kohn, M. Grove, F. J. Ryerson, C. E. Manning, and B. N. Upreti (2001), Geochronologic and thermobarometric constraints on the evolution of the Main Central Thrust, central Nepalese Himalaya, *J. Geophys. Res.*, *106*, 16,177–16,204.

Cattin, R., and J. P. Avouac (2000), Modeling mountain building and the seismic cycle in the Himalaya of Nepal, *J. Geophys. Res.*, *105*, 13,389–13,407.

Colchen, M., P. LeFort, and A. Pêcher (1986), *Annapurn -Manasl -Ganesh Himal*, 136 pp., Cent. Natl. de la Rech. Sci., Paris.

Coleman, M. E., and K. V. Hodges (1998), Contrasting Oligocene and Miocene thermal histories from the hanging wall and footwall of the South Tibetan detachment in the central Himalaya from $^{40}Ar/^{39}Ar$ thermochronology, Marsyandi Valley, central Nepal, *Tectonics*, *17*(5), 726–740.

Copeland, P., T. M. Harrison, K. V. Hodges, P. Maruéjol, P. LeFort, and A. Pêcher (1991), An early Pliocene thermal disturbance of the Main Central Thrust, central Nepal: Implications for Himalayan tectonics, *J. Geophys. Res.*, *96*, 8475–8500.

Crowley, P. D., P. W. Reiners, J. M. Reuter, and G. D. Kaye (2002), Laramide exhumation of the Bighorn Mountains, Wyoming: An apatite (U-Th)/He thermochronology study, *Geology*, *30*, 27–30.

Dalrymple, G. B., and W. A. Duffield (1988), High precision $^{40}Ar/^{39}Ar$ dating of Oligocene rhyolites from the Mogollon-Datil volcanic field using a continuous laser system, *Geophys. Res. Lett.*, *15*(5), 463–466.

Ducea, M., M. A. House, and S. Kidder (2003), Late Cenozoic denudation and uplift rates in the Santa Lucia Mountains, California, *Geology*, *31*, 139–142.

Edwards, R. M. (1995), $^{40}Ar/^{39}Ar$ geochronology of the Main Central thrust (MCT) region: Evidence for late Miocene to Pliocene disturbances along the MCT, Marsyangdi River valley, west-central Nepal Himalaya, *J. Nepal Geol. Soc.*, *10*, 41–46.

Ehlers, T. A. (2005), Crustal thermal processes and the interpretation of thermochronometer data, *Rev. Miner. Geochem*, *58*, 315–350.

Fitzgerald, P. G., and A. J. W. Gleadow (1988), Fission-track geochronology, tectonics and structure of the Transantarctic Mountains in Northern Victoria Land, Antarctica, *Chem. Geol.*, *73*, 169–198.

Foster, D. A., and A. Gleadow (1996), Structural framework and denudation history of the flanks of the Kenya and Anza Rifts, East Africa, *Tectonics*, *15*(2), 258–271.

Gansser, A. (1964), *Geology of the Himalayas*, 289 pp., Wiley-Intersci., Hoboken, N. J.

Hames, W. E., and S. A. Bowring (1994), An empirical evaluation of the argon diffusion geometry in muscovite, *Earth Planet. Sci. Lett.*, *124*, 161–167.

Hodges, K. V. (2000), Tectonics of the Himalaya and southern Tibet from two perspectives, *Geol. Soc. Am. Bull.*, *112*, 324–350.

Hodges, K. V. (2003), Geochronology and thermochronology in orogenic systems, in *The Crust*, edited by R. L. Rudnick, pp. 263–292, Elsevier, New York.

Hodges, K. V., J. M. Hurtado, and K. X. Whipple (2001), Southward extrusion of Tibetan crust and its effect on Himalayan tectonics, *Tectonics*, *20*(6), 799–809.

Hodges, K., C. Wobus, K. Ruhl, T. Schildgen, and K. Whipple (2004), Quaternary deformation, river steepening, and heavy precipitation at the front of the Higher Himalayan ranges, *Earth Planet. Sci. Lett.*, *220*, 379–389.

Hodges, K. V., K. W. Ruhl, C. W. Wobus, and M. S. Pringle (2005), $^{40}Ar/^{39}Ar$ geochronology of detrital minerals, *Rev. Miner. Geochem*, *58*, 315–350.

House, M., S. Kelley, and M. Roy (2003), Refining the footwall cooling history of a rift flank uplift, Rio Grande rift, New Mexico, *Tectonics*, *22*(5), 1060, doi:10.1029/2002TC001418.

Jackson, M., and R. Bilham (1994a), Constraints on Himalayan deformation inferred from vertical velocity fields in Nepal and Tibet, *J. Geophys. Res.*, *99*, 13,897–13,912.

Jackson, M. E., and R. Bilham (1994b), 1991–1992 GPS measurements across the Nepal Himalaya, *Geophys. Res. Lett.*, *21*(12), 1169–1172.

Kirby, E., P. W. Reiners, M. A. Krol, K. X. Whipple, K. V. Hodges, K. A. Farley, W. Q. Tang, and Z. L. Chen (2002), Late Cenozoic evolution of the eastern margin of the Tibetan plateau: Inferences from $^{40}Ar/^{39}Ar$ and (U-Th)/He thermochronology, *Tectonics*, *21*(1), 1001, doi:10.1029/2000TC001246.

Koppers, A. (2002), ArArCALC software for $^{40}Ar/^{39}Ar$ age calculations, *Comput. Geosci.*, *28*, 605–619.

Le Fort, P. (1975), Himalayas: The collided range—Present knowledge of the continental arc, *Am. J. Sci.*, *275-A*, 1–44.

Macfarlane, A. M. (1993), The chronology of tectonic events in the crystalline core of the Himalayas, Langtang National Park, central Nepal, *Tectonics*, *12*(4), 1004–1025.

Macfarlane, A., K. V. Hodges, and D. Lux (1992), A structural analysis of the Main Central thrust zone, Langtang National Park, central Nepal Himalaya, *Geol. Soc. Am. Bull.*, *104*, 1389–1402.

Martin, A. L., P. G. DeCelles, G. E. Gehrels, P. J. Patchett, and C. Isachsen (2005), Isotopic and structural constraints on the location of the Main

Central thrust in the Annapurna Range, central Nepal Himalaya, *Geol. Soc. Am. Bull.*, *117*, 926–944.
Pêcher, A. (1989), The metamorphism in the central Himalaya, *J. Metamorph. Geol.*, *7*, 31–41.
Purdy, J. W., and E. Jaeger (1976), K-Ar ages on rock-forming minerals from the central Alps, *Mem. Inst Geol Min. Univ. Padova*, *30*, 31 pp.
Reiners, P. W., T. A. Ehlers, J. I. Garver, S. G. Mitchell, D. R. Montgomery, J. A. Vance, and S. Nicolescu (2002), Late Miocene exhumation and uplift of the Washington Cascade Range, *Geology*, *30*, 767–770.
Reiners, P. W., Z. Zhou, T. A. Ehlers, C. Xu, M. T. Brandon, R. D. Donelick, and S. Nicolescu (2003), Post-orogenic evolution of the Dabie Shan, eastern China, from (U-Th)/He and fission-track thermochronology, *Am. J. Sci.*, *303*, 489–518.
Renne, P. R., C. C. Swisher, A. L. Deino, D. B. Karner, T. Owens, and D. J. DePaolo (1998), Intercalibration of standards, absolute ages and uncertainties in $^{40}Ar/^{39}Ar$ dating, *Chem. Geol.*, *145*, 117–152.
Ruhl, K., and K. Hodges (2005), The use of detrital mineral cooling ages to evaluate steady-state assumptions in active orogens: An example from the central Nepalese Himalaya, *Tectonics*, *24*, TC4015, doi:10.1029/2004TC001712.
Seeber, L., and V. Gornitz (1983), River profiles along the Himalayan arc as indicators of active tectonics, *Tectonophysics*, *92*, 335–367.
Stock, J. D., and D. R. Montgomery (1996), Estimating paleorelief from detrital mineral age ranges, *Basin Res.*, *8*, 317–327.
Stöcklin, J. (1980), Geology of Nepal and its regional frame, *J. Geol. Soc.*, *137*, 1–34.
Thiede, R. C., B. Bookhagen, J. R. Arrowsmith, E. Sobel, and M. Strecker (2004), Climatic control on rapid exhumation along the southern Himalayan front, *Earth Planet. Sci. Lett.*, *222*, 791–806.
Valdiya, K. S. (1980), *Geology of the Kumaun Lesser Himalaya*, 291 pp., Wadia Inst. of Himalayan Geol., Dehra Dun, India.
Wagner, G. A., and G. M. Reimer (1972), Fission track tectonics: The tectonic interpretation of fission track apatite ages, *Earth Planet. Sci. Lett.*, *14*, 263–268.
Wagner, G. A., G. M. Reimer, and E. Jäger (1977), Cooling ages derived by apatite fission track, mica Rb-Sr, and K-Ar dating: The uplift and cooling history of the central Alps, *Mem. Univ. Padova*, *30*, 1–27.
Wobus, C. W., K. V. Hodges, and K. X. Whipple (2003), Has focused denudation sustained active thrusting at the Himalayan topographic front?, *Geology*, *31*, 861–864.
Wobus, C., A. Heimsath, K. Whipple, and K. Hodges (2005), Active out-of-sequence thrust faulting in the central Nepalese Himalaya, *Nature*, *434*, 1008–1011.

K. V. Hodges and K. W. Huntington, Department of Earth, Atmospheric and Planetary Science, Massachusetts Institute of Technology, Cambridge, MA 02139, USA. (kruhl@mit.edu)